Mälardalen University
School of Innovation Design and Engineering
Västerås, Sweden

Thesis for the Degree of Master of Science in Electronics and ICT Engineering Technology

6.0 (University of Antwerp) + 15.0 (Mälardalen University) credits

DEVELOPMENT OF AN INSTRUMENTATION SYSTEM FOR THE CHARACTERISATION OF VELOSTAT MATERIAL

Louis de Looze
lde23001@student.mdu.se

Examiner: Martin Ekström
Mälardalen University, Västerås, Sweden

Supervisors: Saad Abdullah, Abdelakram Hafid
Mälardalen University, Västerås, Sweden

01/06/2023

Abstract

This work proposes the Velostat Development Kit (VDK), a versatile and high-performing instrumentation system to characterise the properties of Velostat, a piezoresistive material widely used in tactile sensor arrays.

The VDK consists of a hardware and software part, where they are both integrated to work seamlessly together. The hardware provides a high-speed switching interface between the electrodes and the Velostat material, as well as all the circuitry needed to conduct the appropriate measurement. The software provides an interface to control the system and returns real-time data to the user. Both parts offer great flexibility for the end-user and the given interfaces allow for user-made extensions, which are both substantial for future research.

The proposed instrumentation system offers a set of functionality that lowers the difficulty to start experimenting with Velostat. Therefore, allowing for further development of biomedical, robotics or entertainment sensors.

Table of Contents

List of Figures

List of Tables

1. Introduction

Tactile sensors measure physical interaction through touch, applied pressure or temperature changes. These sensors often take the form of arrays, which provide a three-dimensional map of the interaction being measured. This map can be used in numerous applications, such as the following examples:

- sleep monitoring (e.g.,[1]);
- posture monitoring (e.g.,[2], [3]);
- floor-based foot pressure measuring (e.g.,[4]);
- shoe insole pressure measuring (e.g.,[5], [6]);
- interactive sensing floors (e.g.,[7]);
- Musical Instrument Digital Interface (MIDI) controllers (e.g.,[8]).

While such arrays are usually expensive, patented, or vendor-dependent, there has been a significant amount of research dedicated to finding alternatives. One such alternative is Velostat, a composite polymer consisting of carbon-impregnated polyethene that exhibits stimuli-dependent electrical conductivity.

This thesis describes the development of an instrumentation system to characterise Velostat, the Velostat Development Kit (VDK). The focus lies on the design and construction of a flexible custom-built test rig with the ability to use any excitation signal and will thereby facilitate research and development in the following domains:

- material layer combinations;
- electrode connecting methods;
- custom excitation signals;
- advanced sensing algorithms;
- bespoke signal processing methods.

Researchers in the aforementioned fields can benefit significantly from this test rig, as it avoids the need to initiate their work from a foundational level.

The design of the proposed instrumentation system is guided by well-established and extensively researched techniques that have demonstrated their efficacy in the field. However, the system is designed to offer enhanced flexibility, allowing for customisation and extension beyond the conventional approaches. This flexibility is achieved by making hardware choices that increase flexibility and performance. Additionally, the interfacing software developed for this system has been meticulously designed to ensure cross-device compatibility, eliminating the need for specific software installations. This design choice facilitates ease of use and enables researchers from diverse backgrounds to readily employ the VDK without encountering unnecessary technical hurdles.

To highlight the system's capabilities and guarantee its usability, a distinct sensing principle has been implemented, complemented by a dedicated visualisation algorithm. This initial implementation serves as a demonstrative showcase of the functionality and opens up possibilities for future research and development within the field of tactile sensing.

2. Background

In this section, we present a concise summary of the key findings derived from our methodological review [9]. To provide an overview of an instrumentation system for tactile sensing, Figure 1 illustrates a diagram depicting the key components. These components serve as focal points for our in-depth investigation into the current status of each element.

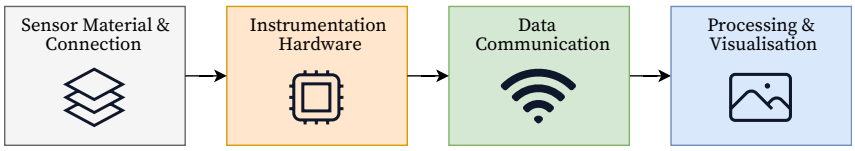

Figure 1: A block diagram visualising all key elements needed for our instrumentation system.

2.1 Sensor Material and Connection

The Velostat material consists of a polymeric foil (polyolefins) impregnated with carbon black. In other words, this makes the material electrically conductive and can consequently be used as a packaging material to protect electronics from electrostatic discharge. According to the original trademark filing by the manufacturer, Custom Materials, this material has no known applications beyond this use [10]. In addition to its conductive characteristics, Velostat belongs to the group of piezoresistive materials, meaning that its resistance changes in response to pressure and latent heat, (i.e., resistance decreases with the increase of pressure). Furthermore, this material has good flexibility, allowing it to be attached to virtually any surface and is therefore frequently used to create sensors. The surface resistivity of Velostat is about 31 $k\Omega/cm^2$. [11]

Since creating a sensor from Velostat was not intended by the manufacturer, the available information in the provided datasheet is scarce. As a result, extensive research has been done by Dzedzickis et al. [12] characterising Velostat and improving our understanding of this material. In brief, their research has been valuable for the understanding of Velostat.

To establish resistance measurements and consequently quantify tactility, it is necessary to establish electrical connections with the Velostat material. There are multiple approaches to achieve this, with the most prevalent method involving the creation of a matrix that divides the Velostat into multiple sensors. In this approach, the tactile resolution is defined by the size of each individual sensor. Another less common technique involves placing electrodes solely around the perimeter of the Velostat and applying an excitation signal to two electrodes. Unlike the matrix approach, this method does not partition the material into multiple sensors but instead utilises the entire sheet for a tactile response. In this work, we will focus on the latter method. A comprehensive overview of all electrode connection methods, highlighting their characteristics, can be found in our methodological review. [9]

When examining the existing literature concerning sensing algorithms and their subsequent excitation signals in the context of perimeter-placed electrodes, two distinct methods can be utilised: Direct Current (DC) [13] and Alternating Current (AC) [14]. These methods exhibit specific practical implications for our application. In Table 1, we present a concise comparison between these two methods, highlighting their key characteristics.

Table 1: Comparison of two tactile sensing methods: Boundary Potential Projection vs. Cross-sectional Mesh.

	Boundary Potential Projection	Cross-sectional Mesh
Principle	Touch disturbs potential distribution in the sheet	Object shunts some current to ground and disturbs the field
Velostat characteristic	Piezoresistivity	Electric conductivity
References	Youzhi Zhang et al. [13]	Yang Zhang et al. [14]
Excitiation signal	Direct Current	Alternating Current
Field form	Orthogonal	Circular
Localisation	✓	✓
Weight classification	✓	✗
Advantages	Relatively easy to implement	Involves the use of advanced processing algorithms
Limitations	Resolution is limited by number of electrodes per unit area	Only works for grounded objects

Direct Current: Boundary Potential Projection

The boundary potential projection method has been extensively researched and successfully implemented by Youzhi Zhang et al. [13]. It works by alternately constructing two direct current (DC) uniform electric fields with orthogonal directions in the piezoresistive film. By measuring the change in boundary potential between the two uniform electric fields, it is possible to accurately determine the location of the contact region in the piezoresistive film. The results of the experiment demonstrate that the sensor can effectively detect the position of contact in real-time and that it has some ability to classify the magnitude of the contact force.

Alternating Current: Cross-sectional Mesh

The researched and very well-documented method by Yang Zhang et al. [14] involves the application of a small alternating current (AC) between a pair of adjacent electrodes, generating an electric field. This process is repeated for all possible combinations of current-projecting and voltage-measuring pairs, thereby creating a mesh of cross-sectional measurements. It should be noted that this technique is only applicable to grounded objects, such as a user's finger, as it shunts some of the current to ground. While this approach can effectively locate a grounded object, its ability to measure pressure remains inconclusive at best.

One major advantage of this technique is that its resolution is not limited by the number of electrodes per unit area. This allows for the possibility of improving tactile resolution through other means in comparison to the previous method.

2.2 Instrumentation Hardware and Communication

Some researchers have utilised Atmel ATmega328-based evaluation boards, such as the Arduino and Lilypad, for their experiments. It has been observed that the ADC in these boards is faster than what is stated in the datasheet, as reported by Open Music Labs [15]. Despite this advantage, the connectivity of these boards can be a limiting factor and thus more powerful microcontrollers are needed. In our previous review, we made a list of microcontrollers with fast ADCs based on Niconiconi's work [16]. Most of the available choices are sufficient and offer a comprehensive set of features.

Depending on the sensor connection method, a multiplexer (MUX) is needed as the number of probes exceeds the analogue inputs. A MUX is a device that selects between several input

signals and forwards the selected input to a single output line and is typically controlled by a set of digital inputs. When choosing a MUX, it is important to consider the number of inputs and outputs required, the data rate, the switching speed, the voltage and current ratings, and the cost. There are many different MUX options available on the market, with varying characteristics and features. For example, the ADG706 [17] and the ADG732 [18] are 16 and 32-channel MUXes, respectively, with fast switching speeds.

In general, there are two types of communication; wireless and wired. During our search for other literature, the communication methods mostly were 2.4GHz based (e.g. transceiver [6], Bluetooth [14], Wi-Fi [19]) and wired (e.g. ethernet [20], USB [21]). Serial communication methods, such as UART, are generally insufficient for transmitting raw sensor data. However, the inclusion of full-speed USB implementation in most microcontrollers allows the transmission of higher data rates.

The type of data being transmitted can significantly impact the choice of communication method. Raw sensor data, for example, will require higher data rates to be transmitted effectively. In cases where data processing is performed on the microcontroller itself, the data rate may be lower due to the added processing time.

2.3 Processing and Visualisation

Data processing is a crucial component in the operation of sensors, however, it falls beyond the scope of this thesis work. Nonetheless, for the sake of completeness, we will provide an overview of various data processing techniques, ranging from straightforward methods to state-of-the-art approaches. A common approach is to first calibrate the sensor using a reference location and pressure, and then apply a smoothing filter to remove noise from the data. Often the resolution from sensor arrays is limited. Jesus et al. [22] have used a resolution enhancement method to enhance the resolution. This method was originally researched by Pradeep Gaidhan [23] and aims to generate a higher-resolution image from multiple lower-resolution images and can also be applied to improve the resolution of sensor arrays. The research conducted by Mutlu et al. [2] focused on the use of machine learning techniques for the classification of sitting posture. The authors demonstrated that their system was able to accurately detect subtle differences in the posture with a high degree of accuracy. Their work highlights the potential of machine learning for sensor array systems.

Most of the other works make use of a single program to do the processing and the visualisation, such as Labview [6], [24] or Matlab [25]. Gala et al. [19] used a web interface based on PHP and MySQL to visualise the data, making it usable from a different device.

3. System Requirements Specification

In this section, we outline the system requirements specification based on the identified shortcomings in the field of tactile sensor systems.

3.1 Functional Requirements

The proposed system must meet a set of functional requirements that are essential for its practical implementation:

Firstly, the system must support different sensing techniques, including specific sensing sequences and injecting signals. Consequently, the hardware components must be carefully selected to offer the necessary flexibility and high performance required for a diversity of sensing approaches. Real-time analysis and interpretation of tactile data should be facilitated, while the interfacing software should provide comprehensive functionality for data analysis, visualisation, and interpretation. Secondly, to ensure accurate and consistent measurements, the system must include a platform designed to securely hold the Velostat material. This minimises any potential variations in connection and position, ensuring reliable and repeatable results. Lastly, every element of the system must be built with a modular architecture, enabling researchers to easily expand and customise the capabilities to fit evolving research needs.

Sensing Principles

Given our objective of developing a highly adaptable instrumentation system, we will tailor our system to best align with both sensing principles from Section 2.1.

In order to integrate the Direct Current: Boundary Potential Projection principle into our instrumentation system, several key requirements must be met. Firstly, we need to generate a uniform electrical feed, two approaches can be considered. The first approach involves physically connecting all electrodes on one side together and doing the same for the opposing side. This configuration ensures a uniform distribution of electric potential across the Velostat surface. Alternatively, a rapid switching mechanism can be implemented, wherein electrodes are switched in succession along a single axis. This approach approximates a uniform electric field and offers a more versatile solution applicable beyond the scope of this specific sensing principle. Secondly, the measuring pairs within the system should be capable to switch between adjacent electrodes. By selectively switching between adjacent electrodes, precise and localised measurements can be obtained. Lastly, the injection signal employed in the system is generated by a constant voltage power source. During a tactile action, the resistance changes and the parameter being measured is the difference in current. To facilitate digital representation and analysis, this current difference needs to be converted into a voltage difference.

The Alternating Current: Cross-sectional Mesh principle operates in a non-orthogonal fashion, employing a mesh style. Both the injecting and measuring pairs of electrodes are positioned adjacently, necessitating the requirement for flexibility of each electrode across the entire Velostat material. If we do not constrain ourselves to adjacent electrode pairs, this would allow alternative sensing principles to be implemented. Furthermore, it is important to consider that, due to the utilisation of AC-current, the circuitry employed must be capable of accommodating such signals. In terms of data visualisation, this principle necessitates the implementation of a distinct visualisation algorithm compared to the previous approach. It is essential to acknowledge that our interfacing software should be developed in a modular fashion, allowing the integration and development of custom algorithms or methods.

3.2 Non-Functional Requirements

The proposed instrumentation system also takes into consideration a set of non-functional requirements that are crucial for its successful implementation:

The system must be designed to be user-friendly and accessible to individuals with varying levels of technical understanding. It ensures that researchers, regardless of their expertise, can effectively utilise the system for their experiments. The user interface and options are designed to provide clear instructions and guidance, making the system easily usable by anyone. Additionally, the system must provide a fixed set of tools that ensure consistency in the measurements. This decreases the time needed to evaluate a future research question in the field of Velostat-based tactile sensors.

3.3 System Interfaces

The following interfaces are essential to ensure efficient functionality and enable future expansion:

Firstly, the system should provide high bandwidth connectivity for real-time data acquisition, processing, and analysis, enabling researchers to develop and evaluate real-time algorithms. Secondly, the system should offer the capability to record data for offline processing. This enables researchers to, for example, pre-train data models and conduct experiments beyond real-time monitoring. Additionally, the system should incorporate standardised connection protocols to ensure future compatibility.

3.4 Verification and Validation

The validation of our system will involve several key steps to ensure its functionality:

Firstly, we will incorporate a mode specifically designed to test direct changes in measurement without any additional processing. This mode will allow us to assess the Velostat's response. Secondly, will include a mode dedicated to testing various sensing principles or processing algorithms. We will evaluate this mode by implementing a specific sensing principle within the system and assessing the system's robustness, accuracy, and responsiveness in various scenarios.

4. Preliminary Testing

Conducting preliminary testing helped in understanding the basic principles of using Velostat as a tactile sensor and served as a starting point for further experimentation and development of our instrumentation system.

As a starting point, I created a uniform electrical field with a potential difference of $2.0\ V$ from left to right. This was accomplished by connecting a variable power supply to the lateral sides with copper tape. The remaining adjacent electrodes were employed for manual measurements. Consistency in the pressure applied on the Velostat was ensured by employing a non-conductive weight. The current differences were converted into a potential difference with the help of an operational amplifier, explained in the section titled "Operational Amplifier" (see 5.2.2). Subsequently, each measurement was normalised to the maximum value of all measuring points and graphically represented by a parabolic curve between the two adjacent measuring points. A baseline measurement is shown in Figure 2a. Altering the position of the object yielded distinct outcomes, represented in Figures 2b, c and d.

Significant manual efforts were spent in acquiring these measurements. Ideally, these would be automated through the utilisation of our instrumentation system. The obtained results unambiguously indicate the potential for the development of a system employing Velostat as a tactile sensor, highlighting its feasibility and promising capabilities.

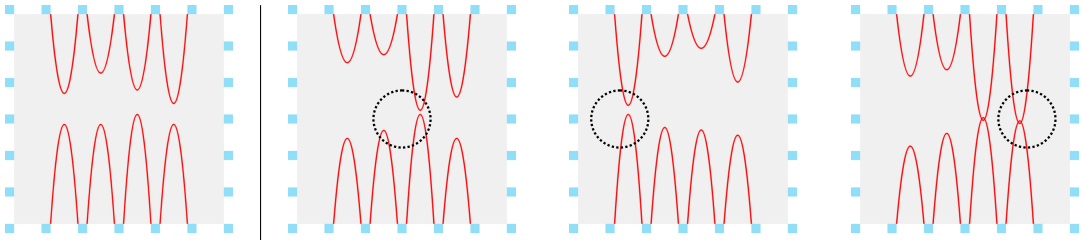

(a) Baseline (b) Center aligned (c) Left aligned (d) Right aligned

Figure 2: Placement alterations of the round non-conductive weight onto the Velostat material while doing unidirectional measurements. The red parabola represents the potential difference between two adjacent points.

5. Design and Implementation

This section aims to provide an overview of the implementation of the Velostat Development Kit (VDK), our instrumentation system. The implementation comprises two critical components, namely the hardware and software aspects, which allow for efficient data generation and analysation. The next sections are based on the key elements of the block diagram in Figure 1.

5.1 Sensor Material and Connection

My connection method was guided by the work of Youzhi Zhang et al. [13], where the Velostat is placed on a custom Printed Circuit Board (PCB). I have increased the number of exposed pads around its perimeter from 16 to 24, which would result in a greater tactile resolution for some sensing principles. The connection between the PCB and the Velostat is done with copper tape and additionally, Kapton tape is used to secure the Velostat onto the PCB. The digital render and actual implementation of the connection method are depicted in Figure 3a and 3b, respectively.

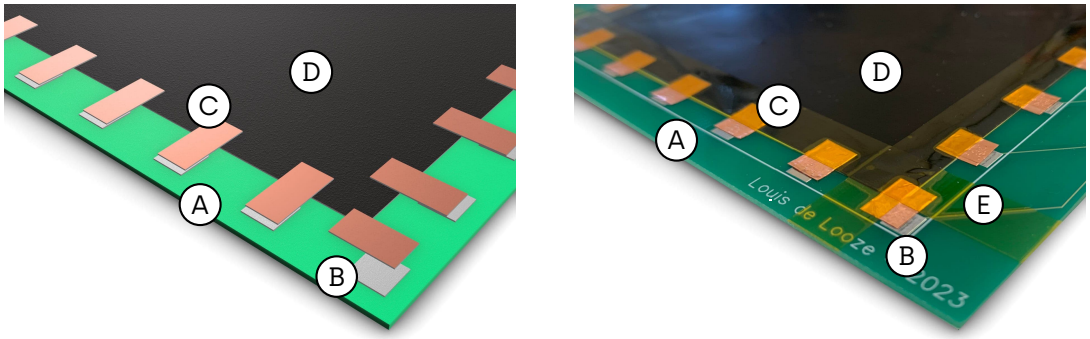

(a) Digital render (b) Physical result

Figure 3: Connection method between PCB and Velostat – Custom PCB (A), electrodes on PCB (B), copper tape to connect Velostat to electrode (C), Velostat material (D), Kapton tape to secure the Velostat (E).

5.2 Instrumentation Hardware and Communication

Our instrumentation system is designed to utilise two pairs of electrodes, namely the projecting and measuring pairs, at any given time. This configuration necessitates the use of four independently controllable multiplexers to select the appropriate electrode pairs. The projecting pair is connected to a power source of choice, while the measuring pair is connected to an Operational Amplifier. This Operational Amplifier is in turn connected to the Analogue to Digital Converter (ADC) of the microcontroller (MCU), which returns a digital representation of the measuring pair.

A complete block diagram of this system is shown in Figure 4.

Multiplexers

The rapid switching between projecting and measuring pairs plays a critical role in our application. Therefore, high-speed analogue multiplexers (MUX) are needed. There are many different MUX options available on the market, each characterised by distinct specifications and functionalities. In our specific case, a minimum of 24 channels is required, and because we need to limit the influence of the switching circuitry; low power dissipation, minimal 'on' resistance, and negligible leakage currents are also required.

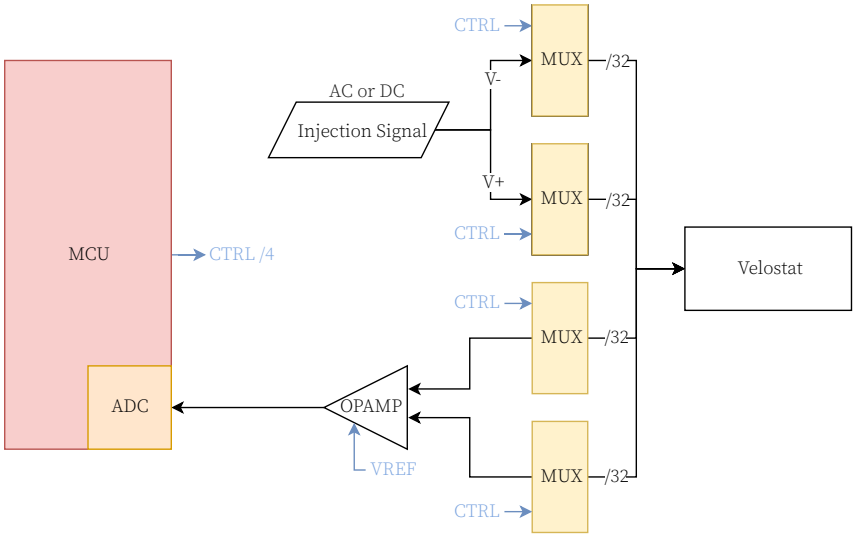

Figure 4: Block diagram of our instrumentation system's hardware.

One notable example is the ADG732 [18], a 32-channel MUX renowned for its fast switching speeds and designed on an enhanced submicron process (see Appendix C), thereby rendering it an optimal choice for our system. We will need to switch between two electrode pairs, resulting in four ADG732s connected to each electrode and positioned on the same PCB close to the Velostat material, visible in Figure 5. The schematic and PCB design can be viewed in Appendix A and B, respectively. Due to the relatively high cost of these switching devices, it is essential to optimise their utilisation. In this context, it is worth noting that out of the 32 data lines available from the MUX, only 24 will be actively employed. To address this issue, a viable solution would be to expand the number of electrodes on the PCB to fully leverage all 32 available electrodes.

Operational Amplifier

During a scanning sequence, our primary objective is to measure the current difference between two points. To achieve this, it is necessary to convert the current into an appropriate voltage, a task typically accomplished through either a voltage divider or an operational amplifier (OpAmp) circuit. The voltage divider is often favoured for its simplicity, as stated by Ramirez et al. in their work [24], where they specifically selected the voltage divider to maintain simplicity. However, the main drawback of this method lies in its non-linear characteristic. Conversely, an OpAmp circuit is linear, although increasing complexity.

During testing, I evaluated both the MAX4208 Evaluation Kit [26] and the TSH82 Configurable OpAmp [27]. The MAX4208 is a precision instrumentation amplifier with variable gain (see Appendix D), defaulting to 148, while the TSH82 is a configurable all-purpose OpAmp (see Appendix E) with a gain of 4.7. Through our testing, I found that the precision amplifier did not yield significantly improved results compared to the all-purpose OpAmp. Therefore, considering factors such as performance and cost, the TSH82 proves to be a more suitable choice for our application.

Microcontroller and Analogue to Digital Converter

The Analogue to Digital converter (ADC) plays a critical role in our system as it facilitates the conversion of the analogue sensor signal into a digital representation. To ensure high-performance ADC capabilities, I conducted a thorough evaluation of multiple microcontroller units (MCUs) featuring fast ADCs (see Section 2.2). Ultimately, I selected the Arduino Portenta H7, which is based on the STM32H7 series (see Appendix F). The chosen Portenta H7 MCU offers impressive

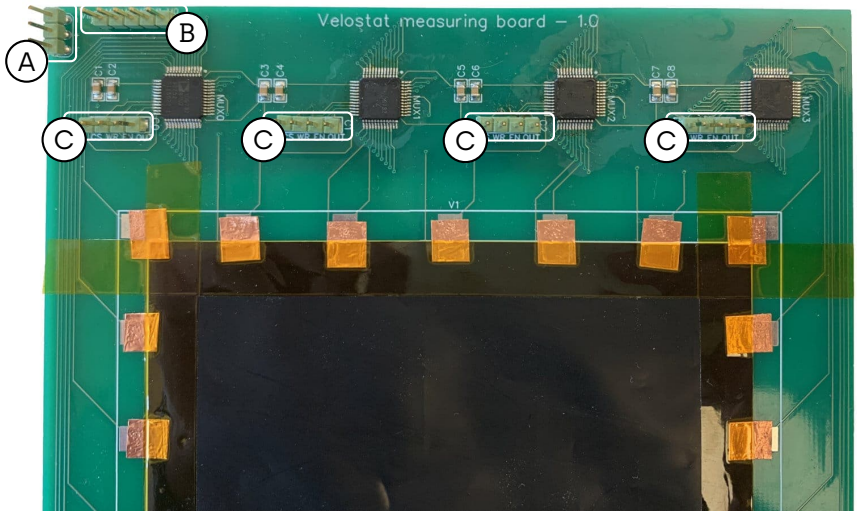

Figure 5: Custom PCB with four ADG732 analogue multiplexers – Power supply connection (A), select pins which are connected to all MUXes (B), control pins and input/output pin for each individual MUX (C).

ADC specifications. It can achieve a maximum sampling rate of 3.6 Msps (Mega samples per second) with a 16-bit resolution, utilising a non-interleaved configuration. Alternatively, with 2x interleaving, it can achieve a sampling rate of 7.2 Msps, still maintaining a 16-bit resolution.

The Portenta H7 also offers other notable advantages that contribute to its suitability for our application. Firstly, this board consists of a high-performance dual-core ARM Cortex-M7 and Cortex-M4 architecture. This would allow us to split up any work over the two cores and therefore speed up the processing. In terms of connectivity, the Portenta H7 is equipped with a microSD card slot, built-in Wi-Fi and Bluetooth modules, Ethernet, and high-speed USB connectivity.

Communication

The communication between the host and device is facilitated through the USB-C Virtual COM Port (VCP) interface, therefore not being limited by UART's slower transfer speeds while still keeping an easy interface to work with. Consequently, the transfer speed is constrained by the USB connection itself.

It is important to note that the VCP operates by transmitting data in chunks with a maximum of 64 bytes. To optimise transmission and processing, I defined a custom packet format that will be used for the communication from device to host. It consists of several essential components, a *preamble*, *from* and *to* pin number, and their corresponding *reading* value. A comprehensive representation of this packet structure is depicted in Figure 6. The adoption of this standardised packet structure ensures seamless integration with other software applications that support serial data ingestion, thereby avoiding unnecessary dependencies or unique drivers. Communication between the host and device primarily involves the exchange of commands and parameters. A comprehensive list of these commands and parameters is provided in Table 2.

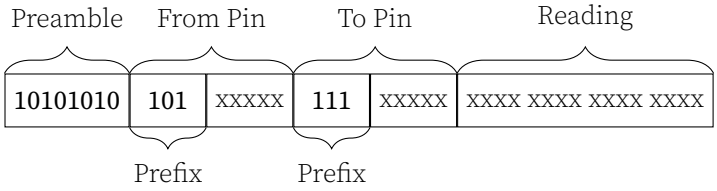

Figure 6: The per-bit packet structure of the transmitted data.

Table 2: An overview of the implemented commands that can be accessed through the serial interface.

Command	Action	Result
i	Enables the Single mode	The device will start measuring and sending data packets.
q	Enables the Sequencer mode	The device will first load the sequence file from SD and then start measuring and sending data packets.
aabbccdd	Defines the electrodes for the Single mode	The parameters a,b,c and d define the ports that need to be enabled for MUX0, MUX1, MUX2 and MUX3 respectively.
r	Start recording	The measured data is stored onto the SD card, allowing offline data processing. (LED on)
s	Stop recording	Data will no longer be written to the SD card. (LED off)

5.3 Processing and Visualisation

In this section, our main focus lies on creating an intuitive and interactive visualisations interface to enhance the understanding and analysis of the acquired data, not on data processing techniques. However, I have implemented some simple algorithms to prove the functionality of the instrumentation system.

To achieve this, I utilised the Svelte framework [28], to develop the interface of the VDK. This web application uses the Web Serial API [29] to connect seamlessly[1] to our physical device. One of the key features of our web interface is its cross-device compatibility, which means that it can be accessed and used on any device, without the need to install special or proprietary software [30]. Additionally, I designed the interface to be intuitive and user-friendly, making it suitable for future researchers independent of their backgrounds.

This interfacing software supports two modes of operation: Single mode and Sequencer mode. The "Single mode" allows the user to manually select the pins to be measured, thereby providing high degrees of flexibility. This mode facilitates real-time monitoring of the current values and displays the previous measurements on a bar graph in averaged bins of one second. On the other hand, the "Sequencer mode" involves retrieving a custom file onto the microSD card that contains a given sequence of ports to be activated. The file consists of a header that includes the character *'q'* followed by a three-digit numeral denoting the total count of entries. Subsequent lines within the document adhere to the command structure denoted as *'aabbccdd'* in Table 2. An extract of such a file is shown in Figure 7b. The data obtained from this mode can be displayed using an appropriate visualisation algorithm. The default algorithm employs parabolic functions to represent the magnitude of voltage differences. Each parabola is accompanied by a corresponding baseline value, which can be manually adjusted or set automatically to the highest value recorded during the duration of this active function. An example reading in the Single and Sequencer mode is shown in Figure 8 and 9, respectively.

To facilitate offline analysis, both modes incorporate a data recorder functionality. This feature allows users to record and store data on the microSD card for further processing and analysis. When starting the recorder, the built-in LED will be enabled. The resulting values in the file are separated by commas and adhere to the following structure $V^+, V^-, V^+_{sen}, V^-_{sen}, measurement$. Examples of this structure are shown in Figure 7a.

This interfacing software is highly customisable and allows for the development of more advanced measurement algorithms and is therefore very useful for future research. The complete flow of interactions between the software and hardware is shown in Figure 10.

[1] As of May 2023, the Web Serial API only works on Chromium-based browsers.

```
0,1,2,3,30519
0,1,2,3,30611
0,1,2,3,30362
0,1,2,3,2500
0,1,2,3,30484
0,1,2,3,11913
...
```

(a) File generated by Recorder

```
q112
00060102
23070102
22080102
21090102
20100102
...
```

(b) File read by Sequencer

Figure 7: An extract of the text files generated and read on the microSD card by the Portenta H7.

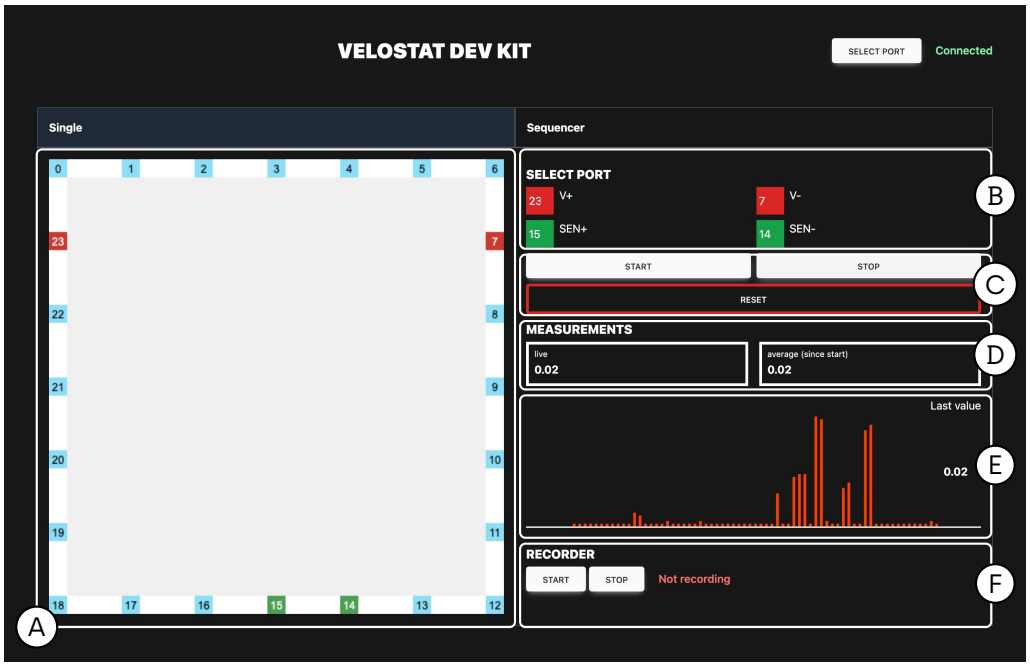

Figure 8: A reading done in the Single mode – The selected electrodes mapped onto the Velostat (A), the selectors to change the electrodes (B), Start or Stop the data processing with the possibility to Reset all the data (C), the potential difference in real-time (D), the potential difference averaged in measurement bins of 1 second (E), the recorder to enable and disable recording to the microSD card (F).

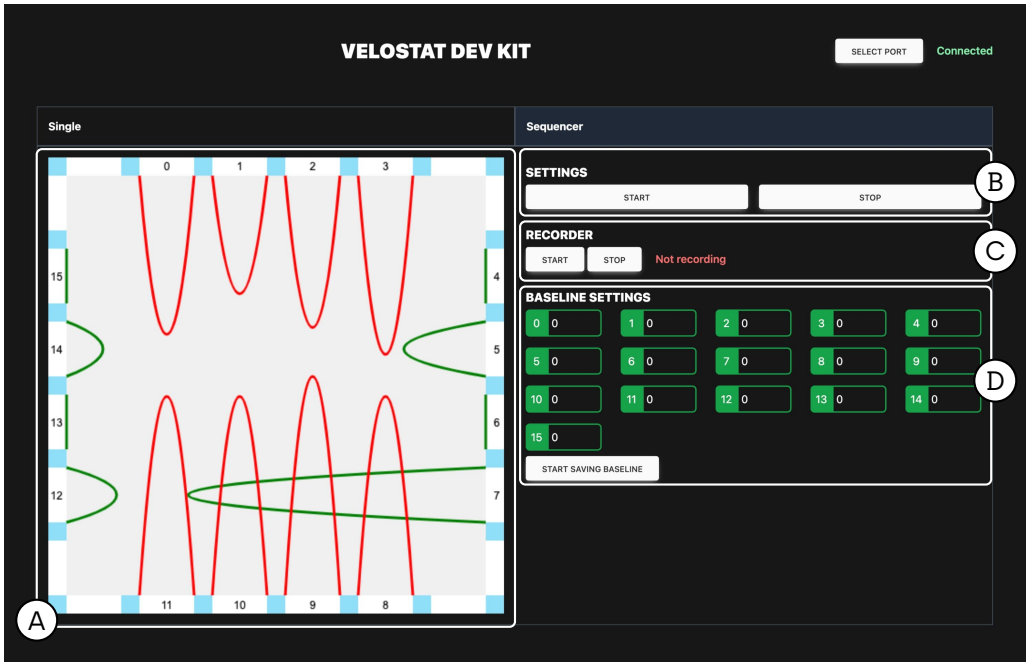

Figure 9: A reading done in the Sequencer mode – The measured potential difference mapped with parabolas onto the Velostat (A), Start or Stop the data processing (B), the recorder to enable and disable recording to the microSD card (C), manually set baseline values or use the button to set them at the current measured values (D).

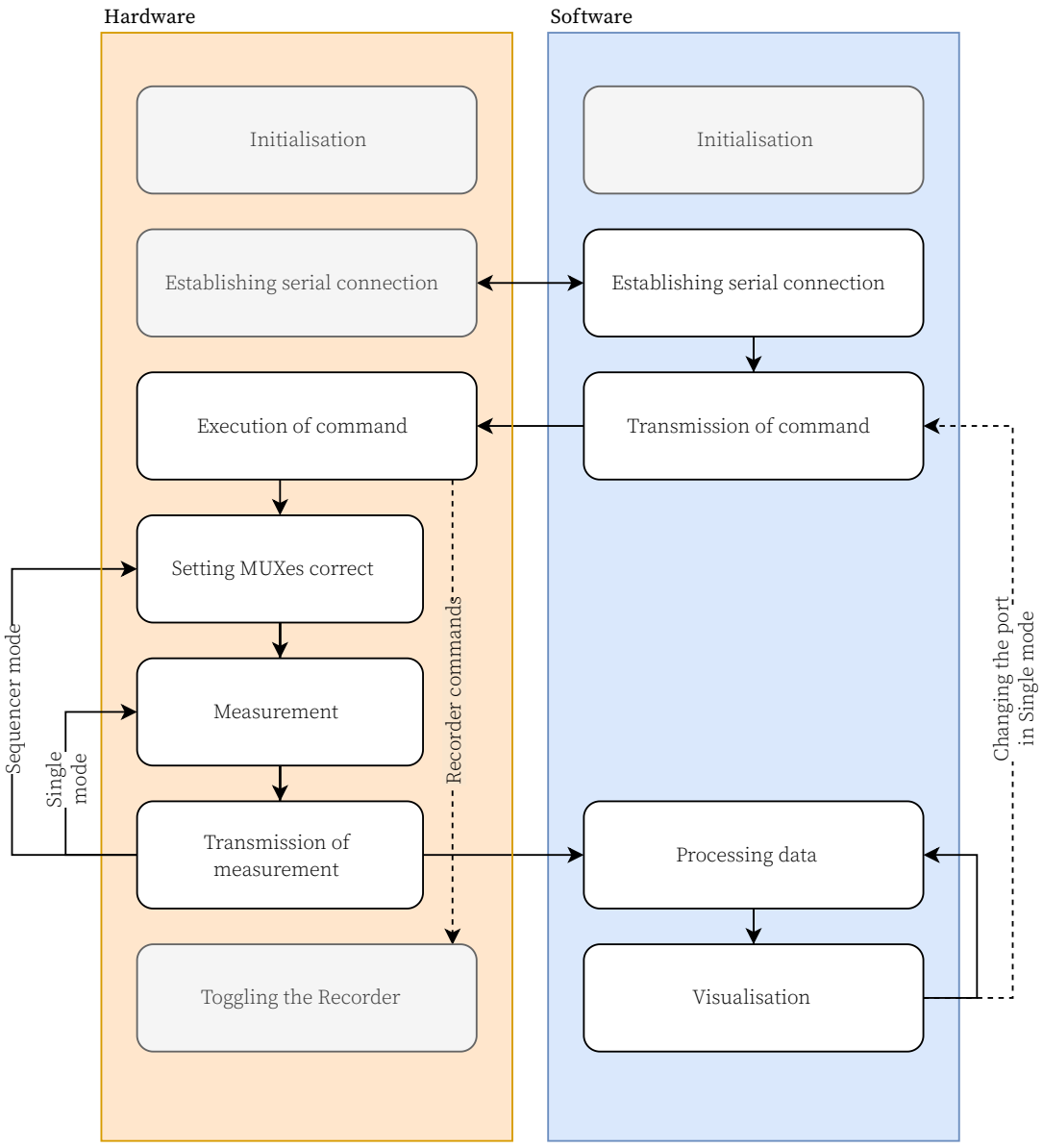

Figure 10: The user-interaction flow of our instrumentation system, showing the interaction between the software and hardware part.

6. Results

In this study, the experimental setup depicted in Figure 11 has been utilised for conducting our tests, and employs the DC-based uniform electric field sensing principle, as described in Section 2.1.1. Throughout the subsequent sections, we will utilise both the Single and Sequencer modes to effectively showcase the capabilities of our instrumentation device. By comprehensively explaining each component, we aim to demonstrate the full potential of the Velostat Development Kit.

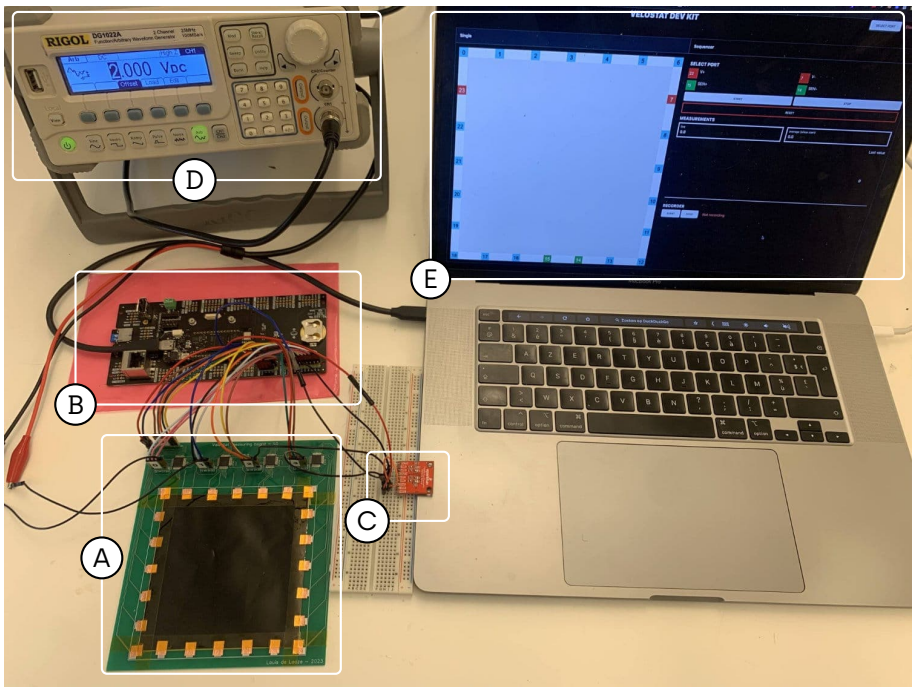

Figure 11: Complete overview of the system – Custom PCB consisting of the Velostat and MUXes (A), Portenta H7 on breakout board (B), TSH82 Operational Amplifier (C), DC-Voltage source (D), Svelte based interfacing software (E).

6.1 Single Mode

To evaluate the Single mode, I configured the port layout as follows: the injecting electrodes were connected to pin 23 and pin 7, while the measuring electrodes were connected to pin 15 and pin 14. The selection of these specific ports was accomplished through my software interface. A visualisation of the electrode locations is presented in Figure 12. Upon initiating the measurement process by pressing the start button, real-time measurements were acquired and shown in a bar graph representation. During this testing phase, I applied three short presses and one long press at location *a*, followed by a single short press at a distinct location *b*. Notably, the potential difference observed at location *b* was significantly smaller compared to that at the initial location. The temporal evolution of the potential difference at each location can be observed in Figure 13.

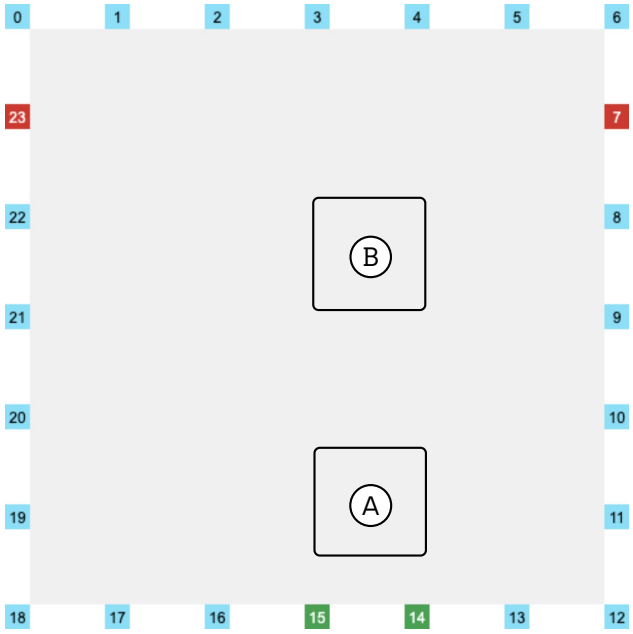

Figure 12: Visual representation of the Velostat material and its electrodes. The red squares indicate the injecting pair, while the green squares represent the measuring pair. The circles labelled as *A* and *B* indicate the locations where pressure was applied during testing.

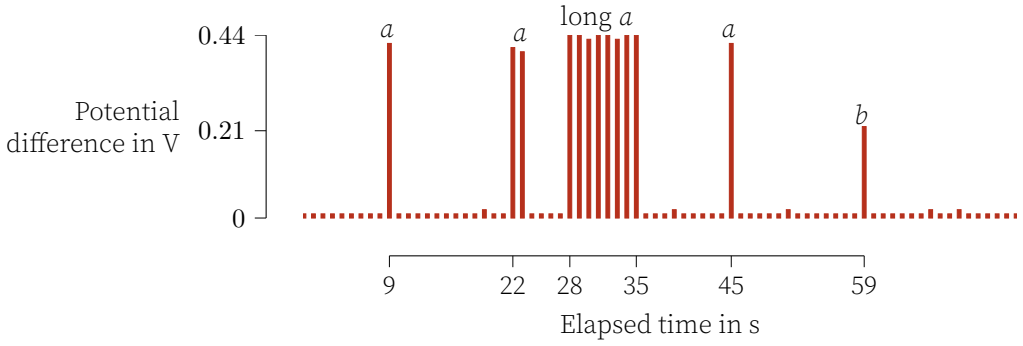

Figure 13: The potential difference, averaged in measurement bins of 1 second, while pressing on positions *a* and *b*.

6.2 Sequencer Mode

In contrast, the sequencer mode provides users with the capability to predefine a sequence of ports. To demonstrate this mode, I have incorporated a preloaded sequence, which can be found in Appendix H. The sequence is based on the Boundary Potential Projection method explained in Section 2.1.1. The sequence begins by establishing a uniform electric field along the x-direction while concurrently measuring the potential difference of adjacent nodes on the opposing sides. This process is then repeated for the y-axis. The measurements obtained are visualised using parabolic representations.

The measurement process was initiated by setting the baseline values, resulting in flat graphs. Thereafter, I applied pressure to two distinct locations, as represented in Figures 14a and 15a. For each location, a sequence of three consecutive frames is presented, originating from my real-time algorithm within the interfacing software.

Regarding the first location, where the point of pressure was applied to the bottom right corner, the three frames can be observed in Figures 14b, c, and d. There is activity in the region of pressure.

For the second location, situated at the centre of the Velostat material, readings were obtained only for all axes in the final frame. This limitation is attributed to the current implementation of the visualisation algorithm, which does not keep track of historic data to validate the new data.

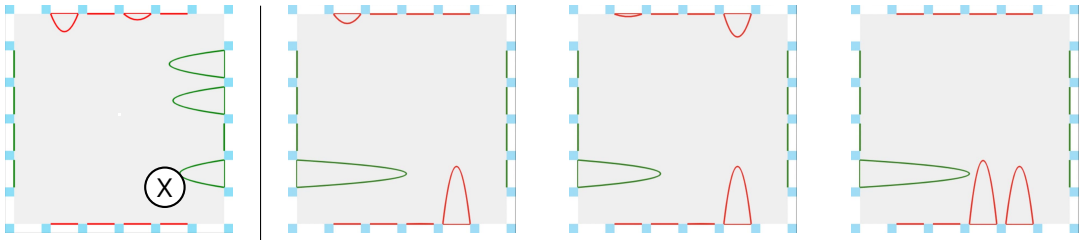

(a) Baseline (b) Frame 1 (c) Frame 2 (d) Frame 3

Figure 14: Testing of the Sequencer mode by applying pressure to the bottom right corner, marked on a. Followed by three consecutive frames that show the evolution of the measurements.

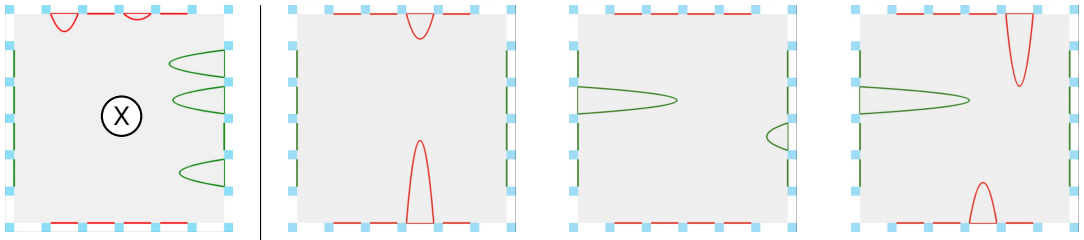

(a) Baseline (b) Frame 1 (c) Frame 2 (d) Frame 3

Figure 15: Testing the Sequencer mode by applying pressure to the centre, marked on a. Followed by three consecutive frames that show the evolution of the measurements.

7. Discussion

Within our System Requirements Specification, we have defined Verification and Validation requirements to ensure the functionality of the Velostat Dev Kit. During the evaluation of the Single Mode, we successfully demonstrated its practicality by effectively detecting changes in the Velostat material without the need for specialised algorithms or extensive data processing. This capability enables us to modify specific variables in the experimental setup and repeat measurements, thereby facilitating further investigation and analysis. Additionally, the testing of the Sequencer Mode provided insights into the performance of our implemented algorithm. However, it revealed certain limitations in visualising various scenarios. Notably, in the bottom left quadrant, we can observe a large parabola that inaccurately suggests proximity to the pressure location. This discrepancy may be attributed to an inadequately calibrated baseline setting, indicating the potential for improvement. Despite the current shortcomings, these findings are promising. Furthermore, the data recorder component was utilised during the verification phase, and it performed following the expected functionality and specifications. In the long run, the Sequencer Mode serves as a valuable platform for the development and refinement of sensing and visualisation algorithms.

Overall, the goals of the thesis were successfully achieved. The VDK demonstrated its usability, flexibility, and extensibility in working with Velostat-based tactile sensors. The validation and evaluation process provided valuable insights into the system's strengths and areas for improvement, guiding future research and development in this field.

At this stage of the project, several aspects could be further expanded upon and improved. Firstly, my implementation does not utilise any onboard data processing capabilities of the proposed hardware. Future work could focus on leveraging these capabilities to enhance the overall performance of the system and thus be more efficient. Secondly, the modular expansion system (see Appendix G) of the Portenta platform would allow us to add expansion headers onto my PCB, simplifying the setup process and enhancing the overall system integration. Lastly, a potential area for improvement lies in the software aspect of the project. By reducing the software overhead, by not using the Arduino stack, the system could potentially achieve higher efficiency. However, this would increase the complexity of the development of new features.

The work conducted in this thesis will significantly contribute to research and development in various domains. Firstly, it will facilitate the experimentation of different material layer combinations, encompassing variations in thickness and the usage of multiple layers to create a multi-layer sensor with a wide variety of material options. Additionally, it will enable the study of various electrode connecting methods, allowing researchers to gain insights into the impact of the results. While the use of copper tape has been proposed, alternative methods can also be explored and evaluated. Furthermore, researchers will have the opportunity to use custom excitation signals, which could result in different stimuli responses. Lastly, the study will foster the development of advanced sensing algorithms and data processing techniques. By integrating these techniques into the system, researchers will be able to improve the accuracy, reliability, and interpretability of the tactile measurements, thereby enabling a more comprehensive and meaningful analysis of tactile information.

8. Conclusion

This thesis introduces the Velostat Development Kit (VDK), an innovative and versatile instrumentation system designed for working with Velostat. This instrumentation system consists of both hardware and software to provide a complete system. The VDK serves as a robust foundation that facilitates research and experimentation across various fields, such as biomedical, robotics or entertainment. Both operating modes of the VDK exhibit exceptional flexibility and extensibility, providing researchers with ample opportunities to customise and expand the system according to their specific requirements.

The conducted sample measurements yielded favourable results, demonstrating the expected functionality and reliability of the VDK. Furthermore, the user-friendly nature of the system allows individuals from various backgrounds to utilise it effectively. The cross-device compatibility further enhances its usability. However, it is important to acknowledge that further development efforts may be necessary to optimise performance and enhance the range of features offered by the VDK.

This thesis represents a significant contribution to the field of Velostat test systems, introducing a powerful tool that fosters advancements in the research and development of Velostat-based tactile sensors.

References

[1] W. Li, C. Sun, W. Yuan, W. Gu, Z. Cui, and W. Chen, "Smart mat system with pressure sensor array for unobtrusive sleep monitoring," *Proceedings of the Annual International Conference of the IEEE Engineering in Medicine and Biology Society, EMBS*, pp. 177–180, Sep. 2017, ISSN: 1557170X. DOI: 10.1109/EMBC.2017.8036791.

[2] B. Mutlu, A. Krause, J. Forlizzi, C. Guestrin, and J. Hodgins, "Robust, low-cost, non-intrusive sensing and recognition of seated postures," *Proceedings of the 20th annual ACM symposium on User interface software and technology - UIST '07*, 2007. DOI: 10.1145/1294211.

[3] B. W. Lee and H. Shin, "Feasibility study of sitting posture monitoring based on piezoresistive conductive film-based flexible force sensor," *IEEE Sensors Journal*, vol. 16, pp. 15–16, 1 Jan. 2016, ISSN: 1530437X. DOI: 10.1109/JSEN.2015.2480600.

[4] S. Corbellini, C. Ramella, C. Fallauto, M. Pirola, S. Stassi, and G. Canavese, "Low-cost wearable measurement system for continuous real-time pedobarography," *2015 IEEE International Symposium on Medical Measurements and Applications, MeMeA 2015 - Proceedings*, p. 639 644, Jun. 2015. DOI: 10.1109/MEMEA.2015.7145281.

[5] R. de Fazio, E. Perrone, R. Velázquez, M. D. Vittorio, and P. Visconti, "Development of a self-powered piezo-resistive smart insole equipped with low-power ble connectivity for remote gait monitoring," *Sensors*, vol. 21, 13 Jul. 2021, ISSN: 14248220. DOI: 10.3390/S21134539.

[6] B. Wang, K. S. Rajput, W. K. Tam, A. K. Tung, and Z. Yang, "Freewalker: A smart insole for longitudinal gait analysis," *Proceedings of the Annual International Conference of the IEEE Engineering in Medicine and Biology Society, EMBS*, vol. 2015-November, pp. 3723–3726, Nov. 2015, ISSN: 1557170X. DOI: 10.1109/EMBC.2015.7319202.

[7] P. Srinivasan, D. Birchfield, G. Qian, and A. Kidané, "A pressure sensing floor for interactive media applications," in *Proceedings of the 2005 ACM SIGCHI International Conference on Advances in Computer Entertainment Technology*, ser. ACE '05, Valencia, Spain: Association for Computing Machinery, 2005, pp. 278–281, ISBN: 1595931104. DOI: 10.1145/1178477.1178526. [Online]. Available: https://doi.org/10.1145/1178477.1178526.

[8] Benyryves, *Eight pressure-sensitive velostat/linqstat pads for a velocity-sensitive midi controller youtube*, [Accessed 2022-12-17]. [Online]. Available: https://www.youtube.com/watch?v=x041YBvLkLs.

[9] L. de Looze, A. Hafid, and S. Abdullahs, "A methodological review of velostat-based tactile sensor arrays."

[10] USPTO, *Velostat trademark status and document retrieval*, [Accessed 2022-11-19]. [Online]. Available: https://tsdr.uspto.gov/#caseNumber=86793440%5C&caseType=SERIAL_NO%5C&searchType=statusSearch.

[11] Adafruit, *Velostat datasheet*, [Accessed 2022-12-17]. [Online]. Available: https://www.farnell.com/datasheets/1815591.pdf.

[12] A. Dzedzickis, E. Sutinys, V. Bucinskas, *et al.*, "Polyethylene-carbon composite (velostat®) based tactile sensor," *Polymers 2020, Vol. 12, Page 2905*, vol. 12, p. 2905, 12 Dec. 2020, ISSN: 2073-4360. DOI: 10.3390/POLYM12122905. [Online]. Available: https://www.mdpi.com/2073-4360/12/12/2905.

[13] Y. Zhang, Z. Lin, X. You, X. Huang, J. Ye, and H. Wu, "A position-sensitive electronic skin based on boundary potential projection theory," *Sensor Review*, vol. 40, no. 1, pp. 130–140, Jan. 2020, ISSN: 0260-2288. DOI: 10.1108/SR-10-2019-0243. [Online]. Available: https://doi.org/10.1108/SR-10-2019-0243.

[14] Y. Zhang, G. Laput, and C. Harrison, "Electrick: Low-cost touch sensing using electric field tomography," in *Proceedings of the 2017 CHI Conference on Human Factors in Computing Systems*, ser. CHI '17, Denver, Colorado, USA: Association for Computing Machinery, 2017, pp. 1–14, ISBN: 9781450346559. DOI: 10.1145/3025453.3025842. [Online]. Available: https://doi.org/10.1145/3025453.3025842.

[15] OpenMusicLab, *Inner workings of the atmega328p adc*, [Accessed 2022-12-17]. [Online]. Available: http://www.openmusiclabs.com/learning/digital/atmega-adc/.

[16] Niconiconi, *List of microcontrollers with fast analog-to-digital converters*, [Accessed 2023-12-17]. [Online]. Available: https://niconiconi.neocities.org/posts/list-of-mcu-with-fast-adc/.

[17] AnalogDevices, *Adg706, low voltage 16 channel multiplexer*, [Accessed 2022-12-17]. [Online]. Available: https://www.analog.com/en/products/adg706.html.

[18] Analog, *Adg732*, [Accessed 2023-03-16]. [Online]. Available: https://www.analog.com/media/en/technical-documentation/data-sheets/ADG726_732.pdf.

[19] M. Gala, J. Barabas, and M. Kopaskova, "User presence monitoring based on velostat pressure sensors and arduino platform," *Proceedings of 2020 IEEE 21st International Conference on Computational Problems of Electrical Engineering, CPEE 2020*, Sep. 2020. DOI: 10.1109/CPEE50798.2020.9238739.

[20] P. Srinivasan, D. Birchfield, G. Qian, and A. Kidané, "A pressure sensing floor for interactive media applications," in *Proceedings of the 2005 ACM SIGCHI International Conference on Advances in Computer Entertainment Technology*, ser. ACE '05, Valencia, Spain: Association for Computing Machinery, 2005, pp. 278–281, ISBN: 1595931104. DOI: 10.1145/1178477.1178526. [Online]. Available: https://doi.org/10.1145/1178477.1178526.

[21] A. M. Rathnayaka, W. N. Perera, H. P. Savindu, *et al.*, "A customized system to assess foot plantar pressure: A case study on calloused and normal feet," *2018 IEEE Region 10 Symposium, Tensymp 2018*, pp. 202–206, Jul. 2018. DOI: 10.1109/TENCONSPRING.2018.8691898.

[22] K. F. D. Jesus, M. H. Cheng, L. Jiang, and E. G. Bakhoum, "Resolution enhancement method used for force sensing resistor array," *Journal of Sensors*, vol. 2015, 2015, ISSN: 16877268. DOI: 10.1155/2015/647427.

[23] P. Gaidhani, *Super-resolution: Generating a higher resolution image from lower resolution images*, [Accessed 2022-12-17]. [Online]. Available: https://homepages.inf.ed.ac.uk/rbf/CVonline/LOCAL_COPIES/AV1011/Super_Resolution_CVonline.pdf.

[24] D. Z. M. Ramirez, M. D. P. G. Souto, B. M. Oldfrey, P. Smitham, M. Miodownik, and C. Holloway, "Characterization of bespoke force sensors for tailored applications," *IEEE Sensors Journal*, vol. 17, pp. 1727–1734, 6 Mar. 2017, ISSN: 1530437X. DOI: 10.1109/JSEN.2016.2644378.

[25] F. Mattar, H. A. Qudaimat, B. A. Qaroot, and M. A. Yaman, "Low cost foot plantar-pressure scanning pad," *Middle East Conference on Biomedical Engineering, MECBME*, vol. 2016 November, pp. 20–24, Nov. 2016, ISSN: 21654255. DOI: 10.1109/MECBME.2016.7745399.

[26] Analog, *Max4208 evaluation kit datasheet*, [Accessed 2023-03-16]. [Online]. Available: https://www.analog.com/media/en/technical-documentation/data-sheets/MAX4208EVKIT.pdf.

[27] ST, *Tsh82*, [Accessed 2023-03-16]. [Online]. Available: https://www.st.com/resource/en/datasheet/tsh80.pdf.

[28] Svelte, *Svelte*, [Accessed 2023-05-16]. [Online]. Available: https://svelte.dev/.

[29] MDN, *Web serial api*, [Accessed 2023-03-16]. [Online]. Available: https://developer.mozilla.org/en-US/docs/Web/API/Web_Serial_API.

[30] L. de Looze, *Velostat development kit interfacing software*, [Accessed 2023-03-16]. [Online]. Available: https://vdk.louisdelooze.be/.

A Schematic for the Printed Circuit Board

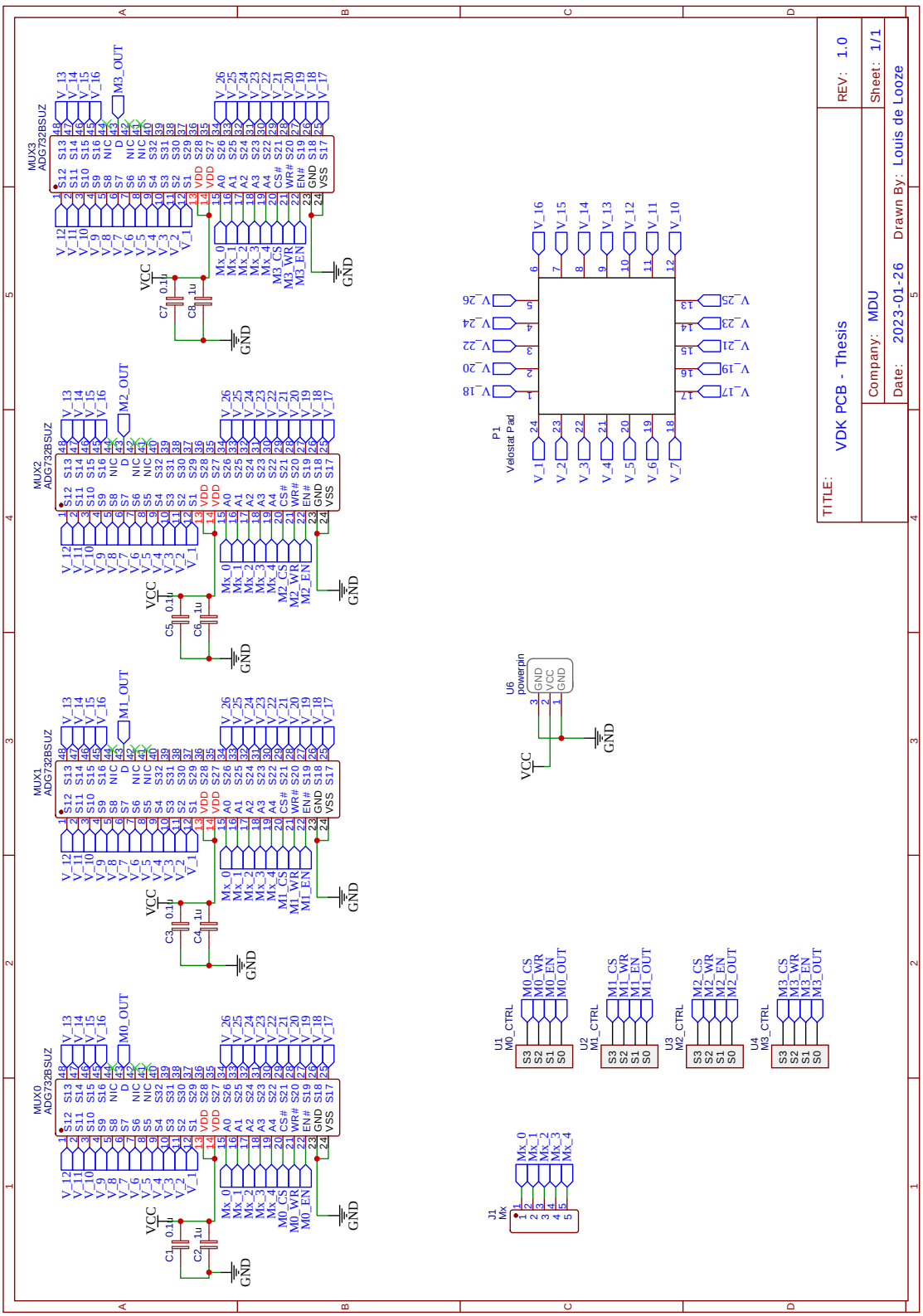

B Printed Circuit Board Layout

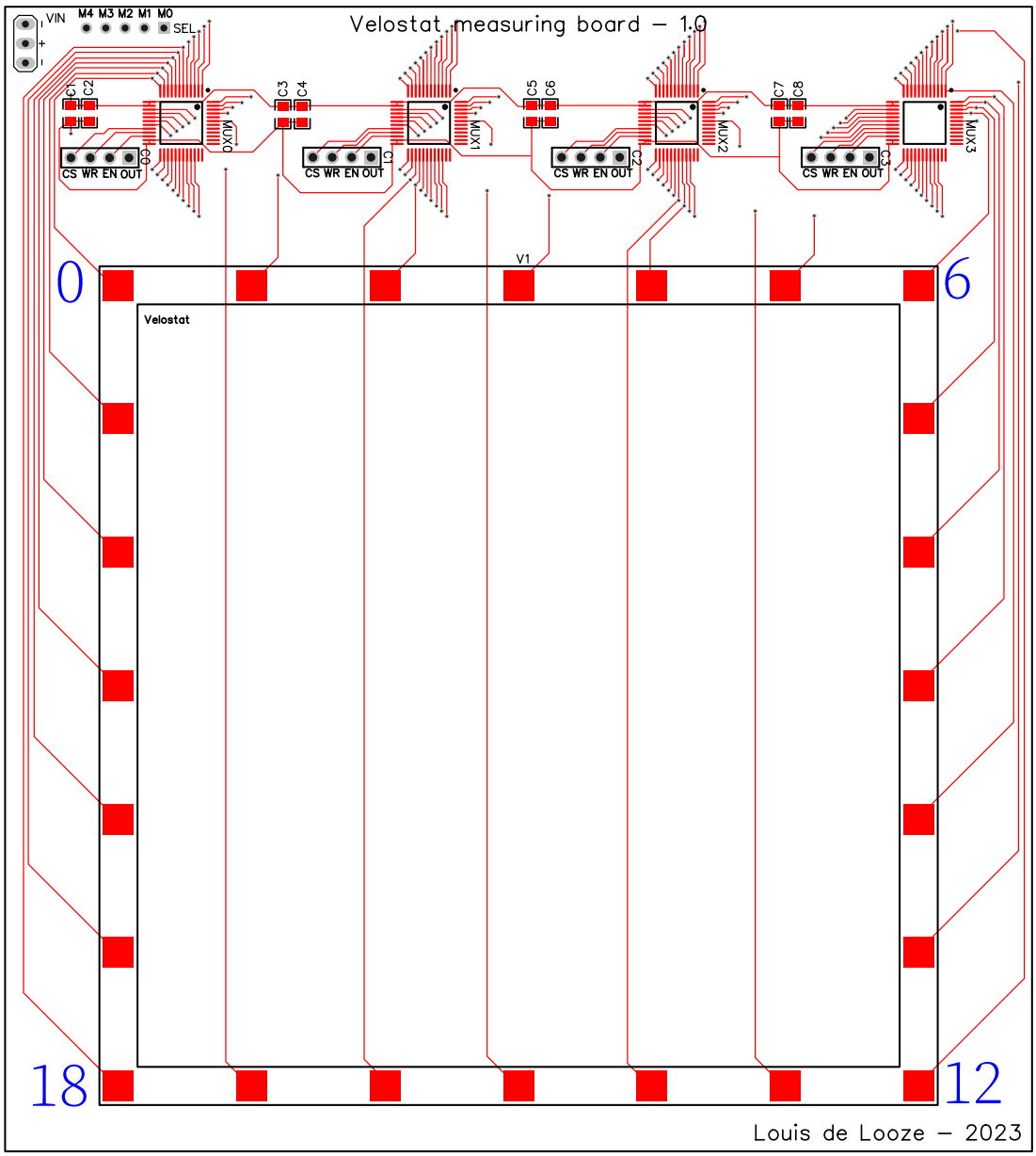

C ADG732: General Description

ANALOG DEVICES

16-/32-Channel, 4 Ω, +1.8 V to +5.5 V and ±2.5 V Analog Multiplexers

Data Sheet **ADG726/ADG732**

FEATURES

- 1.8 V to 5.5 V single-supply operation
- ±2.5 V dual-supply operation
- On resistance: 4 Ω at 25°C (+5 V single supply/±2.5 V dual supply)
- 0.5 Ω on-resistance flatness at 25°C (+5 V single supply/±2.5 V dual supply)
- Rail-to-rail operation
- Transition times: 23 ns typical at 25°C
- Single 32-to-1 channel multiplexer
- Dual/differential 16-to-1 channel multiplexer
- TTL-/CMOS-compatible inputs
- 48-lead TQFP or 48-lead, 7 mm × 7 mm LFCSP

APPLICATIONS

- Optical applications
- Data acquisition systems
- Communication systems
- Relay replacement
- Audio and video switching
- Battery-powered systems
- Medical instrumentation
- Automatic test equipment (ATE)

FUNCTIONAL BLOCK DIAGRAMS

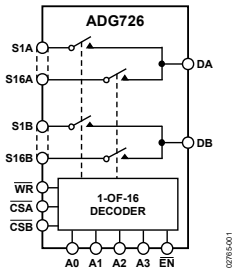

Figure 1.

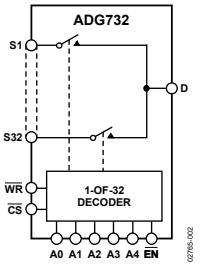

Figure 2.

GENERAL DESCRIPTION

The ADG726/ADG732 are monolithic, complementary metal oxide semiconductor (CMOS) 32-channel and dual 16-channel analog multiplexers. The ADG732 switches one of 32 inputs (S1 to S32) to a common output, D, as determined by the 5-bit binary address lines A0, A1, A2, A3, and A4. The ADG726 switches one of 16 inputs as determined by the 4-bit binary address lines A0, A1, A2, and A3.

On-chip latches facilitate microprocessor interfacing. The ADG726 may also be configured for differential operation by tying $\overline{CSA}$ and $\overline{CSB}$ together. An $\overline{EN}$ input is used to enable or disable the devices. When disabled, all channels are switched off.

These multiplexers are designed on an enhanced submicron process that provides low power dissipation yet gives high switching speed, very low on resistance, and leakage currents. They operate from a single supply of +1.8 V to +5.5 V and a ±2.5 V dual supply, making them ideally suited to a variety of applications. On resistance is in the region of a few ohms and is closely matched between switches and very flat over the full signal range. These devices can operate equally well as either multiplexers or demultiplexers and have an input signal range that extends to the supplies. In the off condition, signal levels up to the supplies are blocked. All channels exhibit break-before-make switching action, preventing momentary shorting when switching channels.

The ADG726/ADG732 are available in a 48-lead LFCSP or a 48-lead TQFP. For functionally equivalent devices with serial interface, see the ADG725/ADG731.

PRODUCT HIGHLIGHTS

1. +1.8 V to +5.5 V single- or ±2.5 V dual-supply operation. These devices are specified and guaranteed with +5 V ± 10%, +3 V ± 10% single-supply, and ±2.5 V ± 10% dual-supply rails.
2. An on resistance of 4 Ω.
3. Guaranteed break-before-make switching action.
4. 48-lead LFCSP package or 48-lead TQFP package.

One Technology Way, P.O. Box 9106, Norwood, MA 02062-9106, U.S.A.
Tel: 781.329.4700
Technical Support www.analog.com

D MAX4208: General Description

19-0997; Rev 0; 9/07

MAXIM

MAX4208 Evaluation Kit

Evaluates: MAX4208/MAX4209

General Description

The MAX4208 evaluation kit (EV kit) simplifies evaluation of the MAX4208 ultra-low offset/drift, adjustable gain, precision instrumentation amplifier in a µMAX® package. The MAX4208 features high-impedance differential inputs optimized for small voltages (±100mV max) and provides rail-to-rail output. The MAX4208 EV kit is configured for a gain of 148V/V. The EV kit operates from a single-supply voltage between 2.85V and 5.5V, or dual supplies providing ±1.425V to ±2.75V.

The MAX4208 EV kit can also be used to evaluate the MAX4209 fixed-gain amplifiers. The MAX4208 IC temperature range is -40°C to +125°C.

The MAX4209 EV kit, available separately, evaluates the 100V/V fixed-gain MAX4209 amplifier without external gain-setting resistors.

Note: To evaluate a MAX4209 IC featuring internal gain-setting resistors, order a MAX4209EVKIT+ or request a free sample of the MAX4209 IC along with the MAX4208EVKIT+. See the *Part Selection Table* for IC ordering information.

Component List

DESIGNATION	QTY	DESCRIPTION
C1, C3	2	10µF ±10%, 10V X5R ceramic capacitors (0805) Murata GRM21BR61A106K KEMET C0805C106K8PAC
C2, C4, C5	3	0.1µF ±10%, 10V X5R ceramic capacitors (0402) Murata GRM155R61A104K KEMET C0402C104K8RACTU
C6, C7	0	Not installed, capacitors (0603)
C8	1	1000pF ±10%, 16V X5R ceramic capacitor (0402) Murata GRM155R61C102K
JU1	1	4-pin header
JU2, JU3	2	2-pin headers
R1	1	1kΩ ±0.1% resistor (0805) IRC PCF-W0805LF-03-1001-B
R2	1	147kΩ ±0.1% resistor (0805) IRC PCF-W0805LF-03-1473-B
R3, R4	2	4.99kΩ ±1% resistors (0603)
R5, R6	0	Not installed, resistors—short (0603)
R7	0	Not installed, resistor (1206)
U1	1	MAX4208AUA+ (8-pin µMAX)
—	3	Shunts
—	1	PCB: MAX4208 Evaluation Kit+

µMAX is a registered trademark of Maxim Integrated Products, Inc.

Features

- **Single- or Dual-Supply Operation**
  2.85V to 5.5V Single-Supply Operation
  ±1.425V to ±2.75V Dual-Supply Operation
- **Adjustable Voltage Gain Configured to 148V/V**
- **Rail-to-Rail Output**
- **Configurable Reference Voltage: Externally or Internally Buffered**
- **Optional Current-Sense Mode**
- **Fully Assembled and Tested**

Ordering Information

PART	TYPE
MAX4208EVKIT+	EV Kit

+Denotes lead-free and RoHS-compliant

Part Selection Table

PART	GAIN (V/V)
MAX4208AUA+	Adjustable
MAX4209TAUA+	10
MAX4209HAUA+	100
MAX4209KAUA+	1000

E TSH82: General Description

life.augmented

TSH80, TSH81, TSH82, TSH84

Wide-band rail-to-rail operational amplifiers with standby function

Datasheet - production data

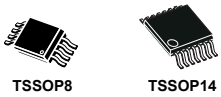

Features

- Operating range from 4.5 to 12 V
- 3 dB-bandwidth: 100 MHz
- Slew rate 100 V/µs
- Output current up to 55 mA
- Input single supply voltage
- Output rail-to-rail
- Specified for 150 Ω loads
- Low distortion, THD 0.1%
- SOT23-5, SO8, and TSSOP packages
- Automotive qualification

Applications

- Video buffers
- A/D converter drivers
- Hi-fi applications

Description

The TSH8x series offers single, dual and quad operational amplifiers featuring high video performance with large bandwidth, low distortion and excellent supply voltage rejection. These amplifiers also feature large output voltage swings and a high output current capability to drive standard 150 Ω loads.

Running at single or dual supply voltages ranging from 4.5 to 12 V, these amplifiers are tested at 5 V (±2.5 V) and 10 V (±5 V) supplies.

The TSH81 device also features a standby mode, which provides the operational amplifier with a low power consumption and high output impedance. This function allows power saving or signal switching/multiplexing for high-speed and video applications.

For board space and weight saving, the TSH8x series is proposed in SOT23-5, SO8, TSSOP8, and TSSOP14 plastic micropackages.

July 2014 DocID009413 Rev 9 1/30

This is information on a product in full production. www.st.com

F Portenta H7 STM-chip: General Description

life.augmented

STM32H747xI/G

Dual 32-bit Arm® Cortex®-M7 up to 480MHz and -M4 MCUs, up to 2MB flash, 1MB RAM, 46 com. and analog interfaces, SMPS, DSI

Datasheet - production data

Features

Includes ST state-of-the-art patented technology

Dual core

- 32-bit Arm® Cortex®-M7 core with double-precision FPU and L1 cache: 16 Kbytes of data and 16 Kbytes of instruction cache; frequency up to 480 MHz, MPU, 1027 DMIPS/ 2.14 DMIPS/MHz (Dhrystone 2.1), and DSP instructions
- 32-bit Arm® 32-bit Cortex®-M4 core with FPU, Adaptive real-time accelerator (ART Accelerator) for internal flash memory and external memories, frequency up to 240 MHz, MPU, 300 DMIPS/1.25 DMIPS /MHz (Dhrystone 2.1), and DSP instructions

Memories

- Up to 2 Mbytes of flash memory with read-while-write support
- 1 Mbyte of RAM: 192 Kbytes of TCM RAM (inc. 64 Kbytes of ITCM RAM + 128 Kbytes of DTCM RAM for time critical routines), 864 Kbytes of user SRAM, and 4 Kbytes of SRAM in Backup domain
- Dual mode Quad-SPI memory interface running up to 133 MHz
- Flexible external memory controller with up to 32-bit data bus: SRAM, PSRAM, SDRAM/LPSDR SDRAM, NOR/NAND flash memory clocked up to 125 MHz in Synchronous mode
- CRC calculation unit

Security

- ROP, PC-ROP, active tamper

General-purpose input/outputs

- Up to 168 I/O ports with interrupt capability

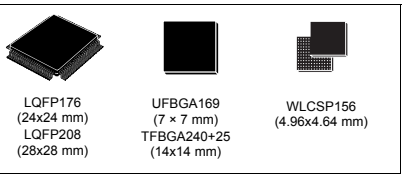

LQFP176 (24x24 mm) LQFP208 (28x28 mm) | UFBGA169 (7 × 7 mm) TFBGA240+25 (14x14 mm) | WLCSP156 (4.96x4.64 mm)

Reset and power management

- 3 separate power domains which can be independently clock-gated or switched off:
  - D1: high-performance capabilities
  - D2: communication peripherals and timers
  - D3: reset/clock control/power management
- 1.62 to 3.6 V application supply and I/Os
- POR, PDR, PVD and BOR
- Dedicated USB power embedding a 3.3 V internal regulator to supply the internal PHYs
- Embedded regulator (LDO) to supply the digital circuitry
- High power-efficiency SMPS step-down converter regulator to directly supply V_{CORE} and/or external circuitry
- Voltage scaling in Run and Stop mode (6 configurable ranges)
- Backup regulator (~0.9 V)
- Voltage reference for analog peripheral/V_{REF+}
- 1.2 to 3.6 V V_{BAT} supply
- Low-power modes: Sleep, Stop, Standby and V_{BAT} supporting battery charging

Low-power consumption

- V_{BAT} battery operating mode with charging capability
- CPU and domain power state monitoring pins
- 2.95 µA in Standby mode (Backup SRAM OFF, RTC/LSE ON)

March 2023 DS12930 Rev 2 1/251

This is information on a product in full production. www.st.com

Clock management

- Internal oscillators: 64 MHz HSI, 48 MHz HSI48, 4 MHz CSI, 32 kHz LSI
- External oscillators: 4-48 MHz HSE, 32.768 kHz LSE
- 3× PLLs (1 for the system clock, 2 for kernel clocks) with Fractional mode

Interconnect matrix

- 3 bus matrices (1 AXI and 2 AHB)
- Bridges (5× AHB2-APB, 2× AXI2-AHB)

4 DMA controllers to unload the CPU

- 1× high-speed master direct memory access controller (MDMA) with linked list support
- 2× dual-port DMAs with FIFO
- 1× basic DMA with request router capabilities

Up to 35 communication peripherals

- 4× I2Cs FM+ interfaces (SMBus/PMBus)
- 4× USARTs/4x UARTs (ISO7816 interface, LIN, IrDA, up to 12.5 Mbit/s) and 1x LPUART
- 6× SPIs, 3 with muxed duplex I2S audio class accuracy via internal audio PLL or external clock, 1x I2S in LP domain (up to 150 MHz)
- 4x SAIs (serial audio interface)
- SPDIFRX interface
- SWPMI single-wire protocol master I/F
- MDIO Slave interface
- 2× SD/SDIO/MMC interfaces (up to 125 MHz)
- 2× CAN controllers: 2 with CAN FD, 1 with time-triggered CAN (TT-CAN)
- 2× USB OTG interfaces (1FS, 1HS/FS) crystal-less solution with LPM and BCD
- Ethernet MAC interface with DMA controller
- HDMI-CEC
- 8- to 14-bit camera interface (up to 80 MHz)

11 analog peripherals

- 3× ADCs with 16-bit max. resolution (up to 36 channels, up to 3.6 MSPS)
- 1× temperature sensor
- 2× 12-bit D/A converters (1 MHz)
- 2× ultra-low-power comparators
- 2× operational amplifiers (7.3 MHz bandwidth)
- 1× digital filters for sigma delta modulator (DFSDM) with 8 channels/4 filters

Graphics

- LCD-TFT controller up to XGA resolution
- MIPI DSI host including an MIPI D-PHY to interface with low-pin count large displays
- Chrom-ART graphical hardware Accelerator (DMA2D) to reduce CPU load
- Hardware JPEG Codec

Up to 22 timers and watchdogs

- 1× high-resolution timer (2.1 ns max resolution)
- 2× 32-bit timers with up to 4 IC/OC/PWM or pulse counter and quadrature (incremental) encoder input (up to 240 MHz)
- 2× 16-bit advanced motor control timers (up to 240 MHz)
- 10× 16-bit general-purpose timers (up to 240 MHz)
- 5× 16-bit low-power timers (up to 240 MHz)
- 4× watchdogs (independent and window)
- 2× SysTick timers
- RTC with sub-second accuracy and hardware calendar

Debug mode

- SWD & JTAG interfaces
- 4-Kbyte embedded trace buffer

True random number generators (3 oscillators each)

96-bit unique ID

All packages are ECOPACK2 compliant

Table 1. Device summary

Reference	Part number
STM32H747 xI	STM32H747AI, STM32H747BI, STM32H747II, STM32H747XI, STM32H747ZI
STM32H747 xG	STM32H747AG, STM32H747BG, STM32H747IG, STM32H747XG

G Portenta H7 High Density Expansion Connectors

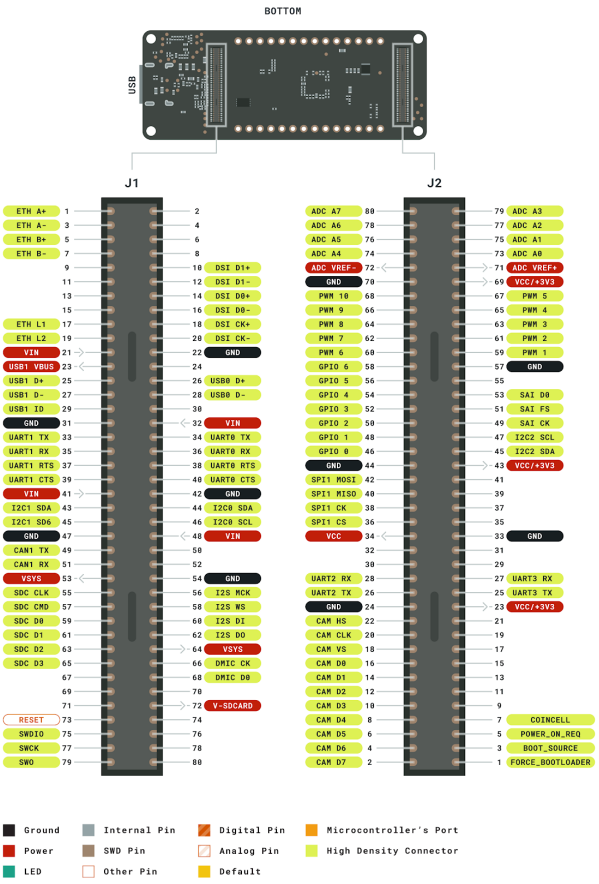

High density connectors pinouts

Pin	Description	Pin	Description
ETH	High Density Connector	CAN	High Density Connector
USB	High Density Connector	DSI	High Density Connector
CAM	High Density Connector	DMIC	High Density Connector
I2C0 I2C1 I2C2I2S	High Density Connector	VSYS VIN V-SDCARDVCC VBUS USB ADC-VREF	Power
GND	Ground	PWM	High Density Connector

H Sequencer File Used for Testing

```
q112
00060102
23070102
22080102
21090102
20100102
19110102
18120102
00060203
23070203
22080203
21090203
20100203
19110203
18120203
00060304
23070304
22080304
21090304
20100304
19110304
18120304
00060405
23070405
22080405
21090405
20100405
19110405
18120405
00061314
23071314
22081314
21091314
20101314
19111314
18121314
00061415
23071415
22081415
21091415
20101415
19111415
18121415
00061516
23071516
22081516
21091516
20101516
19111516
18121516
00061617
23071617
22081617
21091617
20101617
19111617
18121617
00180708
01170708
02160708
03150708
04140708
05130708
06120708
00180809
01170809
02160809
03150809
04140809
05130809
06120809
00180910
01170910
02160910
03150910
04140910
05130910
06120910
00181011
01171011
02161011
03151011
04141011
05131011
06121011
00181920
01171920
02161920
03151920
04141920
05131920
06121920
00182021
01172021
02162021
03152021
04142021
05132021
06122021
00182122
01172122
02162122
03152122
04142122
05132122
06122122
00182223
01172223
02162223
03152223
04142223
05132223
06122223
```